Received: 13 November 2019 | Accepted: 8 March 2020

DOI: 10.1002/jcp.29674

ORIGINAL RESEARCH ARTICLE

Journal of Cellular Physiology WILEY

Frizzled 6 disruption suppresses osteoblast differentiation induced by nanotopography through the canonical Wnt signaling pathway

Rodrigo Paolo Flores Abuna | Fabiola Singaretti Oliveira | Leticia Faustino Adolpho | Roger Rodrigo Fernandes | Adalberto Luiz Rosa | Marcio Mateus Beloti

Bone Research Lab, School of Dentistry of Ribeirão Preto, University of São Paulo, Ribeirão Preto, São Paulo, Brazil

Correspondence
Marcio Mateus Beloti, Bone Research Lab, School of Dentistry of Ribeirão Preto, University of São Paulo, Av. do Café s/n, Ribeirão Preto—SP 14040-904, Brazil.
Email: mmbeloti@usp.br

Funding information
Conselho Nacional de Desenvolvimento Científico e Tecnológico, Grant/Award Number: 303464/2016-0; Coordenação de Aperfeiçoamento de Pessoal de Nível Superior; Fundação de Amparo à Pesquisa do Estado de São Paulo, Grant/Award Numbers: 2016/14171-0, 2016/14711-4 and 2018/17356-6

Disclosure: None.

Abstract

This study aimed to investigate if wingless-related integration site (Wnt) signaling participates in the high osteogenic potential of titanium with nanotopography (Ti-Nano). We showed that among the several components of the Wnt signaling pathway, Frizzled 6 (*Fzd6*) was the transcript most intensely modulated by nanotopography compared with the untreated Ti surface (Ti-Machined). Then, we investigated whether and how *Fzd6* participates in the regulation of osteoblast differentiation caused by nanotopography. The *Fzd6* silencing with CRISPR–Cas9 transfection in MC3T3-E1 cells induced a more pronounced inhibition of osteoblast differentiation of cells cultured on nanotopography than those cultured on Ti-Machined. The analysis of the expression of calcium-calmodulin-dependent protein kinase II and β-catenin demonstrated that *Fzd6* disruption inhibited the osteoblast differentiation induced by Ti-Nano by preventing the activation of Wnt/β-catenin but not that of Wnt/Ca^{2+} signaling, which is usually triggered by the receptor Fzd6. These findings elucidate the biological function of Fzd6 as a receptor that triggers Wnt/β-catenin signaling and the cellular mechanisms modulated by nanotopography during osteoblast differentiation.

KEYWORDS

frizzled, nanotopography, osteoblast, titanium, Wnt

1 | INTRODUCTION

Wingless-related integration site (Wnt) signaling is important in the regulation of several cellular functions, including osteoblast differentiation (Bodine & Komm, 2006). The wnt signaling pathway can be broadly classified into two major subsets, namely, the canonical Wnt signaling, also known as the β-catenin-dependent pathway (Wnt/β-catenin), and its counterpart, the noncanonical Wnt signaling, which includes the planar cell polarity (PCP) and calcium-dependent (Wnt/Ca^{2+}) pathways (Kestler & Kühl, 2008).

In mammals, 19 secreted WNT glycoproteins can bind to 10 Frizzled (FZD) receptors, thus activating downstream signaling. In Wnt/β-catenin signaling, WNT ligands bind to FZDs and the low-density lipoprotein receptor-related protein 5/6 (LRP5/6), followed by the recruitment of disheveled (DVL), which initiates the coclustering of these proteins in signalosomes, triggering LRP6 phosphorylation (Bilic et al., 2007; MacDonald, Tamai, & He, 2009; Monroe, McGee-Lawrence, Oursler, & Westendorf, 2012; van Amerongen, Mikels, & Nusse, 2008). Subsequently, axin is recruited to the cell membrane, producing a dysfunctional destruction complex assembled by several proteins. That phosphorylates β-catenin. Nonphosphorylated β-catenin translocates to the nucleus, where it regulates T-cell factor/lymphoid enhancer-binding factor (TCF/LEF)-dependent transcriptional activation and the key regulators of osteoblast differentiation and maturation (Lerner & Ohlsson, 2015; Monroe et al., 2012).

In noncanonical Wnt signaling, Wnt/Ca^{2+}, the WNT binds to FZDs and recruits DVL and a trimeric G-protein, which activates phospholipase C, triggering diacylglycerol and inositol triphosphate (IP3) formation from the cell membrane. The IP3 binds to its receptor in the endoplasmic reticulum and releases calcium to the cytosol, activating the calcium-calmodulin-dependent protein kinase II (CaMKII) and the nuclear factor of activated T cells (NFAT), which is involved in various cellular functions, including differentiation (Lerner & Ohlsson, 2015; MacDonald et al., 2009).

Wnt signaling has been identified as one of the main signaling pathways regulated by titanium (Ti) surface characteristics, such as topography and wettability (Donos, Retzepi, Wall, Hamlet, & Ivanovski, 2011; Ivanovski et al., 2011; Wall, Donos, Carlqvist, Jones, & Brett, 2009). Nevertheless, whether the canonical or noncanonical Wnt pathway is more important for the interactions between osteoblasts and Ti remains unclear. It seems that the Wnt/β-catenin and Wnt/Ca^{2+} are involved in distinct stages of osteogenic differentiation induced by Ti with microtopography (Olivares-Navarrete, Hyzy, Wieland, Boyan, & Schwartz, 2010). Conversely, Wnt/β-catenin was suggested to be unessential in inducing osteoblast differentiation of cells cultured on this substrate (Olivares-Navarrete et al., 2011). Hence, Wnt/Ca^{2+} might be more important than Wnt/β-catenin, given that WNT11 and WNT5a may work together to mediate the osteoblast commitment of stem cells cultured on nano/microstructured Ti surfaces (Boyan, Olivares-Navarrete, Berger, Hyzy, & Schwartz, 2018).

Nanostructured Ti enhances osteoblast differentiation, which may dictate an improved interfacial bone tissue formation on this surface (De Oliveira, Zalzal, Beloti, Rosa, & Nanci, 2007; Mendonça, Mendonça, Aragão, & Coope, 2008; Rasouli, Barhoum, & Uludag, 2018). Acid etching with H_2SO_4/H_2O_2 solution efficiently generates nanotopography with a pore size of 22 ± 7 nm and exhibits a higher osteogenic potential compared with the untreated Ti surface (Ti-Machined; Castro-Raucci et al., 2016, De Oliveira et al., 2007, Kato et al., 2014, Yi et al., 2006;). We have shown that integrin β3 silencing disrupted the osteoblast differentiation alongside with the downregulation of some components of the Wnt in cells cultured on Ti with nanotopography, suggesting a crosstalk between these pathways that may be linked to the osteogenesis induced of this surface (Lopes et al., 2019). We also observed that the reduction of the signaling triggered by the receptor Fzd4 inhibited the osteoblast differentiation of cells cultured on nanotopography (Abuna et al., 2019). As Wnt/β-catenin and Wnt/Ca^{2+} signaling are of relevance to osteoblast differentiation, in the present study, we aimed to evaluate the participation of Wnt signaling in the high osteogenic potential of Ti-Nano and which of these two pathways is more influential in this process.

2 | MATERIALS AND METHODS

2.1 | Ti surface generation

Ti discs were prepared as described elsewhere (De Oliveira et al., 2007, Yi et al., 2006). Briefly, Ti discs were machined (Ti-Machined) and kept under agitation for 4 hr with a solution of 10 N H_2SO_4 and 30% aqueous H_2O_2 (1:1 vol/vol) to create the nanostructured surface (Ti-Nano) and both surfaces were analyzed using a scanning electron microscope (SEM; Inspect S50, FEI, Hillsboro, OR).

2.2 | Osteoblast cultures

The MC3T3-E1 sub-clone 14 cells (American Type Culture Collection, Manassas, VA) were grown in α-MEM (Invitrogen, Grand Island, NY) with 10% fetal bovine serum (Gibco, Grand Island, NY) and 1% penicillin–streptomycin (Gibco), herein referred to as growth medium, until 80% confluence. The cells were then collected and cultured on Ti discs at a cell density of 10,000 cells/cm^2 in osteogenic medium, which was the growth medium plus 50 μg/ml ascorbic acid (Gibco) and 7 mM β-glycerophosphate (Sigma-Aldrich, St. Louis, MO) for a period of up to 14 days. The medium was changed every other day, and except where indicated that the cells were kept in the growth medium, the experiments were conducted with cells grown in osteogenic medium.

2.3 | Transcriptional analysis by quantitative real-time polymerase chain reaction (RT-qPCR)

The transcriptional expression of selected genes was analyzed by RT-qPCR. Total RNA was extracted from cells cultured on both surfaces and later from the selected cell clones grown on Ti-Nano with Trizol reagent (Invitrogen, Carlsbad, CA). The complementary DNA template was synthesized with the reverse transcription kit (Kit High Capacity; Invitrogen) using 1 μg extracted RNA. Then, RT-qPCR (n = 3) was done with a TaqMan PCR Master Mix (Applied Biosystems, Foster City, CA) and probes for the target genes in Step One Plus Real-Time PCR system (Invitrogen). All transcripts were normalized to ß-actin based on the cycle threshold method ($2^{-\Delta\Delta C_t}$).

2.4 | Frizzled 6 (*Fzd6*) indels mediated by CRISPR–Cas9

2.4.1 | CRISPR–Cas9 vector and guide RNA (gRNA) design

An all-in-one plasmid CRISPR–Cas9–green fluorescent protein (GFP) encoding *Fzd6* gene exon 3-specific gRNA with the sequence TTCATGTAGTTCTACCCTGT was purchased from Sigma-Aldrich (Chromosome: GRCm38: 15: 39,006,034–39,038,188). The 20 base-pair gRNA was selected through an online platform (https://benchling.com) to identify the highest on-target and the lowest probability of the off-target gRNA based on a score established elsewhere (Hsu et al., 2013).

2.4.2 | MC3T3-E1 cell transfection with CRISPR–Cas9 plasmid

Cells were thawed, cultured in the growth medium, and plated (10,000 cells/cm^2) into six-well polystyrene plates. After 24 hr and at 70% confluence, the cells were transfected using the CRISPR–Cas9–Fzd6-mutated (*gFzd6*)–GFP plasmid and its control CRISPR–Cas9–GFP. The plasmids were transfected at a concentration of 2.5 μg/well-using Lipofectamine 3000 reagent (Invitrogen).

2.4.3 | Sorting of single GFP$^+$ cells

The GFP$^+$ cells were isolated through a FACS Aria III flow cytometer (Becton Dickinson, Franklin Lakes, NJ) using BD FACSDiva™ software (Becton Dickinson), and the data were analyzed with FlowJo LLC software v10.5.3. Briefly, after 30 hr of transfection with CRISPR–Cas9–gFzd6–GFP and CRISPR–Cas9–GFP plasmids, the cells were collected and centrifuged at 600*g* for 5 min and the pellets were resuspended with 5 ml growth medium. Nontransfected cells were used as GFP$^-$ control. GFP$^+$ single cells were sorted directly into the individual wells of 96-well plates (Corning Incorporated) containing the growth medium and kept for approximately 5 weeks. The surviving clones were sequentially plated into a 24-well, 6-well plate, and 25 cm^2 culture flask (Corning Incorporated). At 90% confluence, the cells were detached with ethylenediaminetetraacetic acid 0.02% in phosphate-buffered saline (Gibco) and cryopreserved at −80°C for further analysis.

2.4.4 | Identification of mutated clones by western blotting

The western blotting analysis was carried out in accordance with a conventional protocol. FZD6 protein detection was performed in all clones that survived GFP$^+$ cell sorting, including cells transfected with the empty vector (control) and those transfected with specific gRNA (*gFzd6*), in a polyvinylidene difluoride membrane (Bio-Rad, Hercules, CA). For FZD6 detection, a primary rabbit polyclonal anti-FZD6 antibody (ab98933, 1:1,000; Abcam, Cambridge, MA) was used. Only one clone displayed an appropriate disruption of FZD6 protein. This clone was Sanger-sequenced, and the mutation type was identified for use in the next experiments. The runt-related transcription Factor 2 (RUNX2) was identified with primary rabbit monoclonal antibody anti-RUNX2 (8486S, D1H7, 1:1,000; Cell Signaling, Danvers, MA). Phosphorylated CAMKII was identified with a primary rabbit polyclonal anti-CAMKII beta gamma delta antibody (ab182647, phospho T287, 1:1,000; Abcam), whereas total β-catenin with a primary rabbit monoclonal anti-β-catenin antibody (8480S, D10A8, 1:1,000; Cell Signaling). For all proteins, a secondary anti-rabbit immunoglobulin G antibody (7074S, 1:4,000; Cell Signaling) was used, and the control was glyceraldehyde 3-phosphate dehydrogenase (GAPDH) protein, detected with a primary rabbit polyclonal anti-GAPDH antibody (sc25778, 1:1,000; Santa Cruz Biotechnology, Santa Cruz, CA).

2.5 | Extraction of nuclear and cytoplasmic fractions

Nuclear and cytoplasmic proteins were extracted with NE-PER Nuclear and Cytoplasmic Extraction Reagent kit (Pierce Biotechnology, Rockford, IL) according to the manufacturer's instructions and stored at −80°C for western blotting assays.

2.6 | Immunolocalization of CAMKII and phosphorylated β-catenin proteins

The CAMKII and phosphorylated β-catenin proteins were evaluated by indirect immunofluorescence with the primary rabbit monoclonal antibody anti-CAMKII (1:200; Abcam) and primary rabbit polyclonal antibody anti-phosphorylated β-catenin (4176S, Ser675, 1:50; Cell Signaling), followed by a mixture of the red-fluorescent Alexa Fluor 594-conjugated goat anti-mouse secondary antibody (A31623, 1:200; Molecular Probes, Eugene, OR). Green fluorescent Alexa Fluor 488-conjugated phalloidin was used to detect the actin cytoskeleton (A12379, 1:200; Molecular Probes). Nuclei were detected with blue fluorescent DAPI (D3571, 1:300; Molecular Probes). Four Ti-Nano discs were observed and randomly photographed in five areas per disc ($n = 20$) with an epifluorescence light microscope Axio Imager M2 Zeiss (Carl Zeiss, Inc. Göttingen, GO, GE).

2.7 | In situ alkaline phosphatase (ALP) activity and extracellular matrix mineralization

In situ ALP activity was analyzed in *gFzd6* and control cells cultured in osteogenic medium on Ti-Nano using a Fast Red-TR reagent (Sigma-Aldrich), and extracellular matrix mineralization was assessed through calcium content evaluation using Alizarin Red S (Sigma-Aldrich). The samples were examined and photographed with an epifluorescence light microscope Axio Imager M2 Zeiss (Carl Zeiss, Inc.). The in situ ALP and mineralization assay results were measured by pixel quantification on three discs of Ti-Nano considering five random areas per disc ($n = 15$) using the ImageJ 1.52 software (National Institutes of Health). The results were expressed as a percentage of measured regions.

2.8 | Statistical analysis

The data were submitted to one-way analysis of variance and posttest Student–Newman–Keuls or Student's *t* test ($p \leq .05$) and the experiments were done for a minimum of three times.

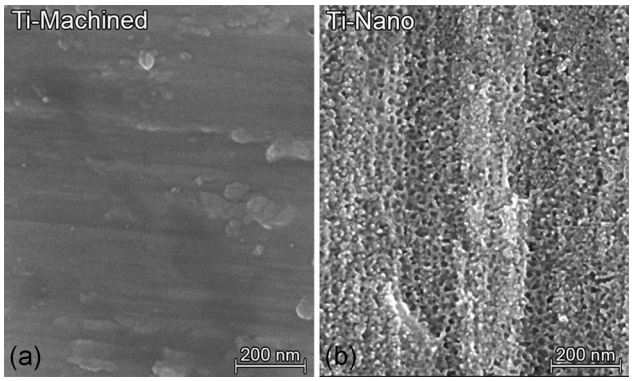

FIGURE 1 Topography of the evaluated Ti surfaces. High-resolution scanning electron micrograph of Ti-Machined (a) and Ti-Nano (b). Ti-Nano, titanium with nanotopography

3 | RESULTS

3.1 | Ti characterization

The evaluation of topography by SEM demonstrated the relatively smooth surface of Ti-Machined (Figure 1a) compared with the unique characteristic of Ti-Nano (Figure 1b) with nanocavities produced by acidic treatment.

3.2 | Effect of Ti-Nano on the messenger RNA (mRNA) expression of elements of the Wnt signaling and osteoblast transcription factors

The expressions of the majority of Wnt-related genes and both transcription factors *Runx2* and *Osx* were upregulated by Ti-Nano on Days 3 and 5 compared with those on Day 7, as observed in the heatmap (Figure 2a). Among the evaluated genes involved in the Wnt signaling pathway, *Fzd6* (Figure 2a,b) was the most modulated by Ti-Nano compared with Ti-Machined on Days 3 ($p = .001$), 5 ($p = .001$), and 7 ($p = .003$).

3.3 | Sorting of GFP$^+$ MC3T3-E1 cells transfected with CRISPR–Cas9

Cells were transfected with a vector expressing GFP, Cas9, and the gRNA-targeting *Fzd6* exon 3 (Figure 3a). After 24 hr, 10,000 cells were sorted by flow cytometry, obtaining 301 GFP$^+$ cells (Figure S1), from which 45 clones were recovered to verify the presence of mutations in *Fzd6* exon 3.

3.4 | Mutated clone *gFzd6* downregulated mRNA and protein expression of FZD6

Our results revealed different effects on FZD6 protein expression in the recovered clones (Figure S2). The clone selected for this study

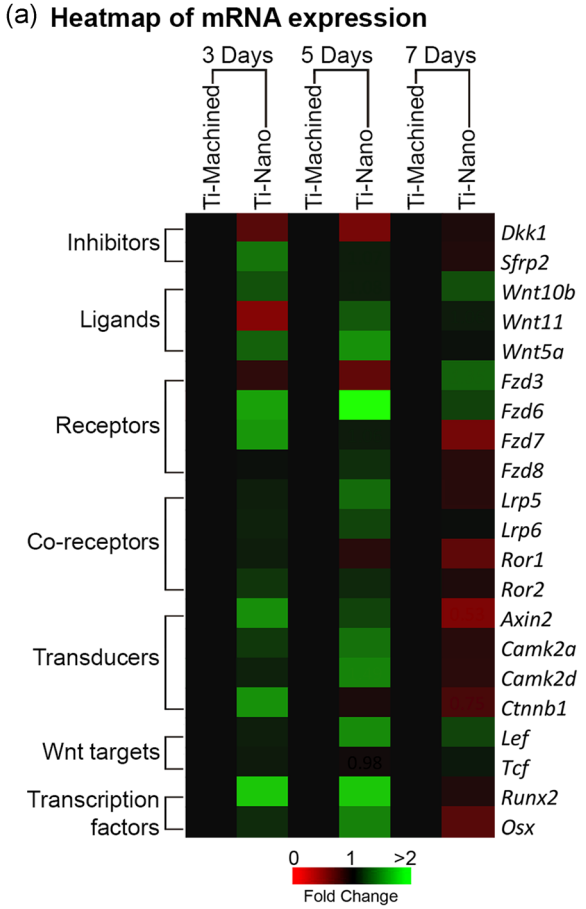

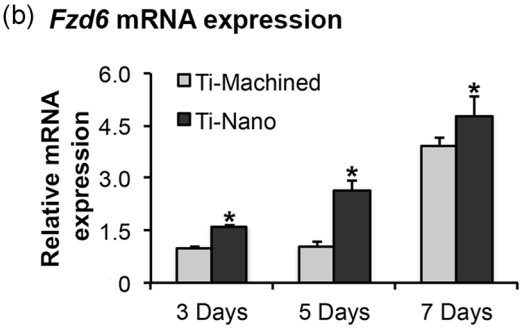

FIGURE 2 Effect of Ti-Nano on the mRNA expression of components of the Wnt signaling pathway and osteoblast transcription factors. Heatmap of the mRNA expressions of *Dkk1*, *Sfrp2*, *Wnt10b*, *Wnt11*, *Wnt5a*, *Fzd3*, *Fzd6*, *Fzd7*, *Fzd8*, *Lrp5*, *Lrp6*, *Ror1*, *Ror2*, *Axin2*, *Camk2a*, *Camk2d*, *Ctnnb1*, *Lef*, *Tcf*, *Runx2*, and *Osx* in MC3T3-E1 cells grown on Ti-Machined and Ti-Nano on Days 3, 5, and 7 (a) and analyzed by RT-qPCR. *Fzd6* mRNA expression in MC3T3-E1 cells grown on Ti-Machined and Ti-Nano on Days 3, 5, and 7 (b). Data on *Fzd6* mRNA expression (b) are presented as mean ± standard deviation ($n = 3$). Asterisks (*) indicate a statistically significant difference between Ti-Machined and Ti-Nano at each time point ($p \leq .05$). mRNA, messenger RNA; Ti-Nano, titanium with nanotopography

was named as *gFzd6*, and it was confirmed as a carrier of an indel mutation affecting one allele of *Fzd6* exon 3 (Figure S3), which downregulated the mRNA (Figure 3b, $p = .001$) and protein (Figure 3c, $p = .001$) expression of FZD6 on Day 3. Furthermore, on

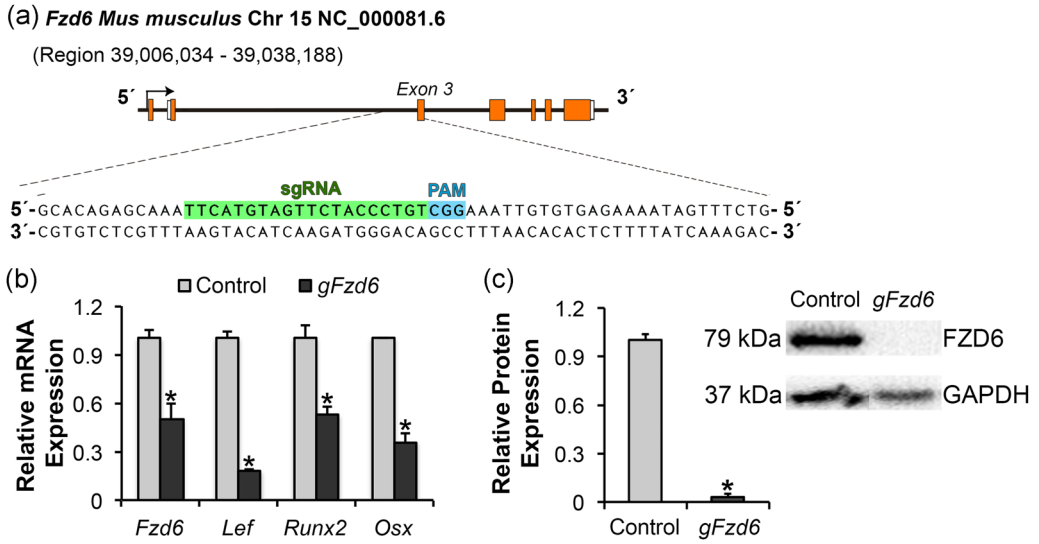

FIGURE 3 Efficiency of CRISPR–Cas9 indel mutations in silencing FZD6. Design of guide RNA for *Fzd6* exon 3 (a), mRNA expression of *Fzd6*, *Lef*, *Runx2*, and *Osx* in MC3T3-E1 *gFzd6* and control cells on Day 3 (b), and protein expression of FZD6 in *gFzd6* and control cells on Day 3 (c). Data on mRNA are presented as mean ± standard deviation ($n = 3$). Asterisks (*) indicate a statistically significant difference between control and *gFzd6* cells ($p \leq .05$). FZD, frizzled; mRNA, messenger RNA; Runx2, runt-related transcription Factor 2

Day 3, this mutation reduced the mRNA expression (Figure 3b) of the Wnt target *Lef* ($p = .001$) and that of osteoblast transcription factors *Runx2* ($p = .001$) and *Osx* ($p = .001$).

3.5 | Effect of *Fzd6* disruption on osteoblast differentiation of cells cultured on Ti-Nano

To investigate whether *Fzd6* silencing displays different effects on cells grown on Ti-Machined and Ti-Nano in terms of osteoblast differentiation, we evaluated Runx2 mRNA and protein expression on Day 5. Although the mRNA and protein expressions of Runx2 were downregulated after *Fzd6* silencing on both surfaces, such reduction was more prominent in cells cultured on Ti-Nano (Figure S4). Given these findings, further experiments were carried out with Ti-Nano only. On Day 3, with the exception of the mRNA expression of *Runx2*, which was unaffected ($p = .202$) by *Fzd6* silencing (Figure 4a), all the other mRNA expressions, *Osx* ($p = .003$), *Alp* ($p = .001$), *Col1a1* ($p = .002$), and *Bsp* ($p = .001$) were downregulated after *Fzd6* silencing of MC3T3-E1 cells cultured on Ti-Nano (Figure 4a). On Day 5, all evaluated mRNA expressions, *Runx2*, *Osx*, *Alp*, *Col1a1*, and *Bsp* were downregulated ($p = .001$ for all) after *Fzd6* silencing of cells cultured on nanotopography (Figure 4b).

On Days 3 and 5, the expression of RUNX2 protein was reduced after *Fzd6* silencing of *gFzd6* cells cultured on nanotopography (Figure 5a). On Day 3, the expression was 76.8% lower ($p = .001$), and on Day 5, it was 66.6% lower ($p = .008$) in *gFzd6* cells compared with the control cells (Figure 5a). On Day 10, in situ ALP activity was reduced (Figure 5b) after *Fzd6* silencing in *gFzd6* cells cultured on Ti-Nano ($p = .002$, 45%), and on Day 14, the formation of the extracellular mineralized matrix (Figure 5c) was also reduced after *Fzd6* silencing of *gFzd6* cells grown on Ti-Nano ($p = .001$, 78%). Given that the amount of mineralized matrix may be affected by cell proliferation, we counted the cells on Days 3 and 5. The reduced extracellular matrix mineralization observed after *Fzd6* silencing in *gFzd6* cells grown on Ti-Nano could not be related to the lower number of cells, given that *Fzd6* silencing did not reduce the number of cells in the evaluated periods (Figure S5).

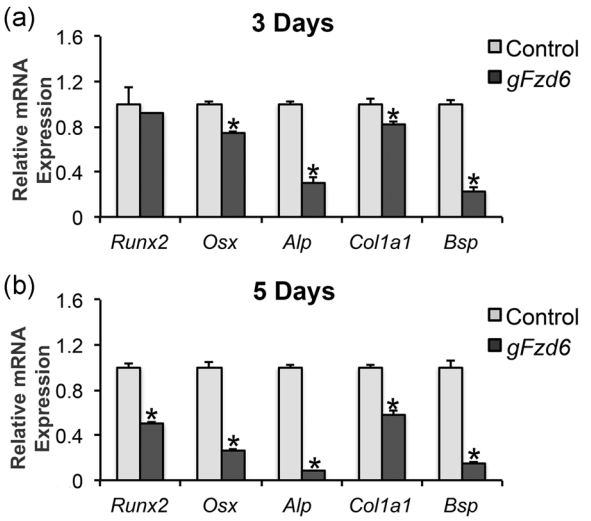

FIGURE 4 Effect of *Fzd6* silencing on the mRNA expression of osteoblast markers of cells grown on Ti-Nano. mRNA expressions of *Runx2*, *Osx*, *Alp*, *Col1a1*, and *Bsp* in MC3T3-E1 *gFzd6* and control cells grown on Ti-Nano on Days 3 (a) and 5 (b). Data are presented as mean ± standard deviation ($n = 3$). Asterisks (*) indicate statistically significant difference between control and *gFzd6* cells ($p \leq .05$). FZD, frizzled; mRNA, messenger RNA; Runx2, runt-related transcription Factor 2

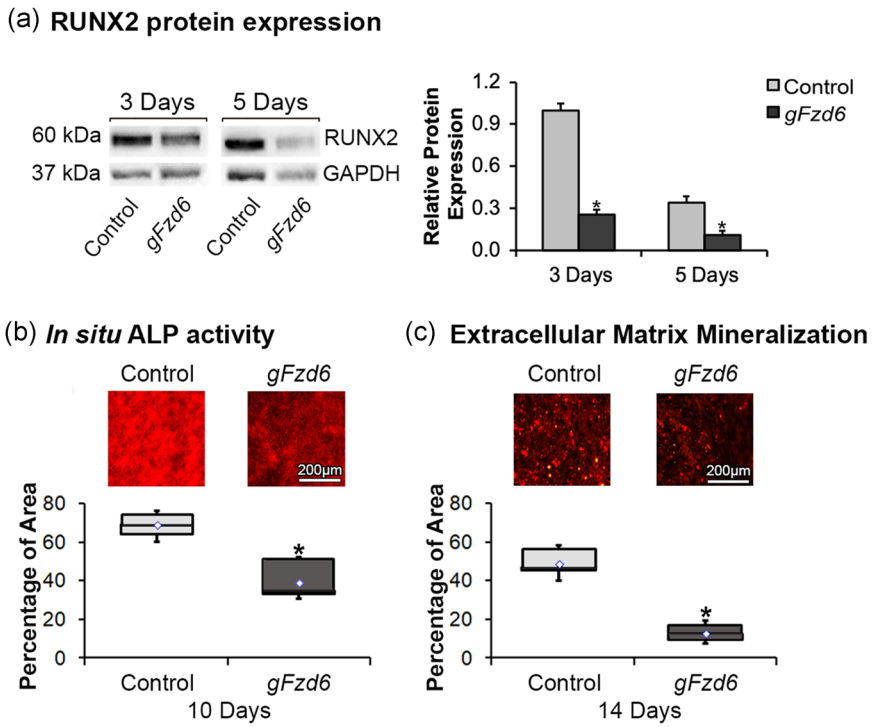

FIGURE 5 Effect of *Fzd6* silencing on the expression of osteoblast phenotype in cells grown on Ti-Nano. Protein expression of RUNX2 on Days 3 and 5 (a), in situ ALP activity on Day 10 (b), and extracellular matrix mineralization on Day 14 (c) in MC3T3-E1 *gFzd6* and control cells grown on Ti-Nano. Data on in situ ALP activity ($n = 15$) and extracellular matrix mineralization ($n = 15$) are presented as box plots. Asterisks (*) indicate a statistically significant difference between control and *gFzd6* cells ($p \leq .05$). ALP, alkaline phosphatase; FZD, frizzled; RUNX2, runt-related transcription Factor 2; Ti-Nano, titanium with nanotopography

3.6 | Effect of *Fzd6* disruption on Wnt/Ca^{2+} signaling pathway in cells cultured on Ti-Nano

On Day 3, *Fzd6* silencing induced the higher protein expressions of CaMKII, phospho-CaMKII, and *Nfatc1* mRNA in *gFzd6* compared with the control cells grown Ti-Nano (Figure 6). Thus, the effect of nanotopography is not due to the Wnt/Ca^{2+} signaling, as initially thought. The protein expression of phospho-CaMKII showed no statistical difference in both *gFzd6* and control cells cultured on Ti-Nano on Days 3 ($p = .665$) and 5 ($p = .161$; Figure 6a). On Day 3, the protein expression of CaMKII, which was indirectly measured by fluorescence intensity, was higher in *gFzd6* cells cultured on nanotopography ($p = .001$) compared with that of the control cells (Figure 6b). The mRNA expression of *Nfatc1* (Figure 6c) was higher in *gFzd6* compared with that of the control cells grown on Ti-Nano on Day 3 ($p = .003$) but not on Day 5 ($p = .541$). Altogether, these data suggest that the Wnt/Ca^{2+} signaling pathway was not responsible for the detrimental effect induced by *Fzd6* silencing on osteoblast differentiation of MC3T3-E1 cells.

3.7 | Effect of *Fzd6* disruption on Wnt/β-catenin signaling pathway in cells cultured on Ti-Nano

Given that the *Fzd6* silencing caused no disruption in the Wnt/Ca^{2+} signaling in cells cultured on nanotopography, we also investigated the effect of this type of silencing on the Wnt/β-catenin signaling pathway (Figure 7). On Days 3 and 5, the expression of total β-catenin was lower by 66% ($p = .024$) and 51.4% ($p = .045$), respectively, in *gFzd6* than in control cells grown on Ti-Nano (Figure 7a). On Day 3, the expression of phospho-β-catenin was higher ($p = .001$) in *gFzd6* compared with that in the control cells grown on Ti-Nano (Figure 7b). Finally, we confirmed that *Fzd6* silencing modulated the translocation of β-catenin from cytoplasm to the nucleus. On Day 3, the reduction of β-catenin in the cytoplasmic ($p = .013$) and nuclear ($p = .008$) fractions of *gFzd6* cells, with more pronounced reduction in the nuclear fraction compared with the control cells, (Figure 7c) revealed that the inhibition of osteoblast differentiation induced by *Fzd6* silencing was due to the disruption of the Wnt/β-catenin signaling pathway.

4 | DISCUSSION

In this study, we used CRISPR–Cas9-mediated mutations to silence one of the Wnt receptors, *Fzd6*, to investigate the participation of Wnt signaling pathway in the well-known high osteogenic potential of a unique Ti surface with nanotopography Surprisingly, *Fzd6* disruption inhibited the osteoblast differentiation caused by nanotopography by preventing the activation of the Wnt/β-catenin signaling pathway but not that of Wnt/Ca^{2+}, which is the pathway usually triggered by Fzd6 receptor.

We detected remarkable differences in the temporal expression of mRNA related to the Wnt pathway in osteoblasts cultured on nanotopography, in which the Wnt signaling is relevant during all phases of culture development. In murine calvaria, *Fzd2* and *Fzd6* transcripts were highly expressed in proliferating primary osteoblasts, and interestingly, these gene expressions decreased in wild-type and

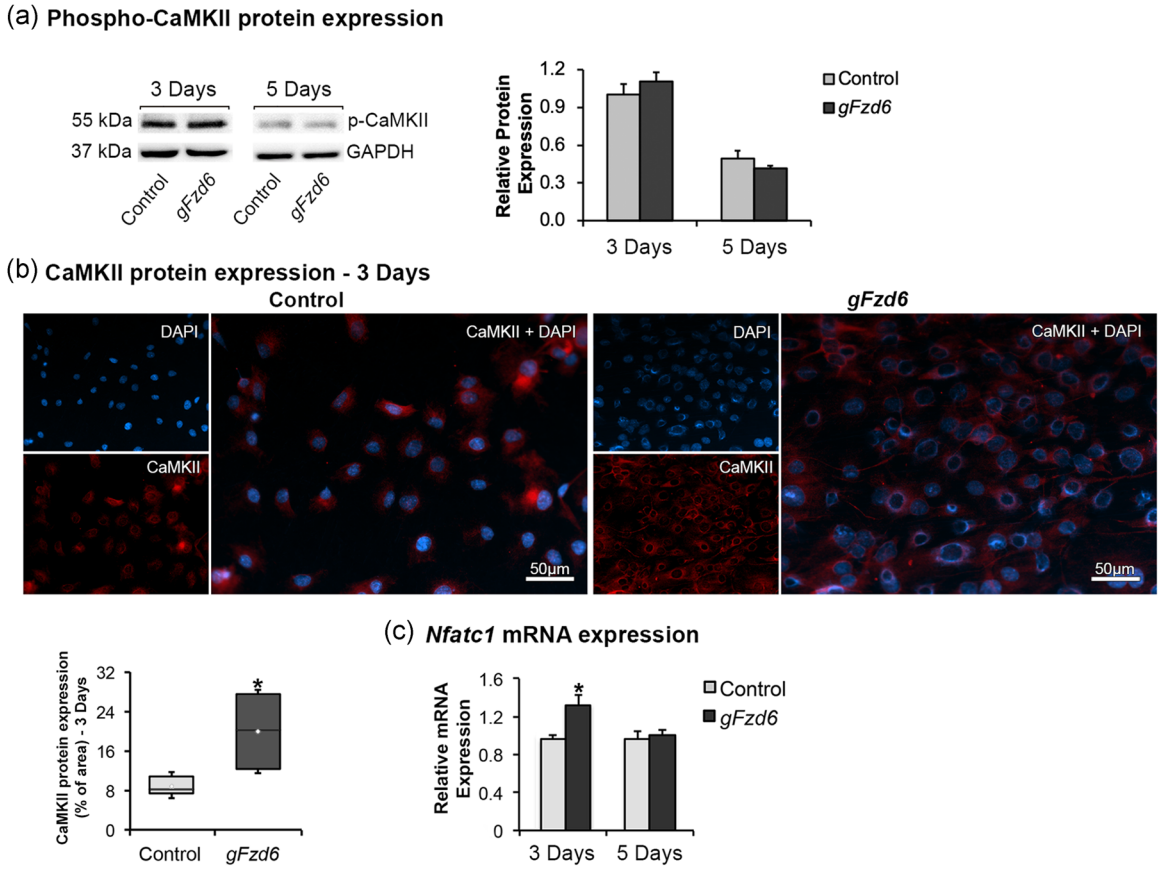

FIGURE 6 Effect of *Fzd6* silencing on the Wnt/Ca^{2+} signaling pathway in cells grown on Ti-Nano. Protein expression of phospho-CaMKII on Days 3 and 5 (a), CaMKII on Day 3 (b) and mRNA expression of *Nfact1* on Days 3 and 5 (c) in MC3T3-E1 *gFzd6* and control cells grown on Ti-Nano. Data on protein expression of CaMKII ($n = 18$) are presented as box plots, and mRNA expression of *Ncfat1* ($n = 3$) are presented as mean ± standard deviation. Asterisks (*) indicate statistically significant difference between control and *gFzd6* cells ($p \leq .05$). (b) Red fluorescence indicates CaMKII, and blue fluorescence denotes cell nuclei (DAPI). FZD, frizzled; mRNA, messenger RNA; Ti-Nano, titanium with nanotopography

Lrp5$^{-/-}$ osteoblasts cultured under osteogenic conditions (Kato et al., 2002). Coincidently, our results showed that Ti-Nano increased *Lrp5* gene expression at early time points of culture growth. Given that in *Lrp5*$^{-/-}$ animals, 50% of the mitotic ratio is reduced, and cell viability is unaffected, *Lrp5* may improve early osteoblast proliferation (Dong et al., 1998; Kato et al., 2002). Although a mutation in the carboxy terminus of LRP5 protein inhibits the transcription of *Wnt3a* in osteoblast cell lines, Lrp5-deficient primary calvarial osteoblasts continually transmit signals independently of *Lrp5*, suggesting that other Wnt receptors, FZD and LRP6, are sufficient to activate the Wnt signaling pathway (Carron et al., 2003; Gong et al., 2001; Kato et al., 2002; Mao et al., 2001). Thus, given that most of the studies on osteoblast response to Ti surfaces used Wnt agonists or antagonists, the evaluation of a specific receptor silencing might be accurate to establish the relevance of Wnt signaling in the interactions between osteoblasts and Ti.

Here, we observed that the most intensely modulated mRNA by Ti-Nano was *Fzd6*, which is usually linked with the Wnt/PCP pathway (Golan, Yaniv, Bafico, Liu, & Gazit, 2004; Heinonen, Vanegas, Lew, Krosl, & Perreault, 2011). The mutations of *Fzd6* are associated with the orientation of hair follicles, inner-ear sensory cells, and neural tube closure (Frojmark et al., 2011; Naz et al., 2012; Wang, Guo, & Nathans, 2006). Nevertheless, the consequences of *Fzd6* mutation on osteoblast behavior on the Ti-Nano substrate are still unknown. Therefore, we used the CRISPR–Cas9 system to mutate exon 3 of *Fzd6* gene, which may affect not only the transcriptional activity of this gene but also interrupt the ligand-receptor interaction given that the designed gRNA targets the cysteine-rich domain, affecting amino acid residues at the 92–94 positions of FZD6 protein (Janda, Waghray, Levin, Thomas, & Garcia, 2012; Lee et al., 2015).

The generation of a knockout strain by a CRISPR–Cas9 system depends on a small random deletion produced by nonhomologous end-joining at the repair site after cleavage of the double DNA strand. These deletions are ideally directed to open reading frames, resulting in frameshifts, the formation of a premature stop codon, and consequent loss of protein function (Gilbert et al., 2013). Conversely, mutations occur randomly and may not alter the reading phase of mRNA (in-frame deletion), maintaining the function of the protein. Given that the ultimate goal was the generation of an FZD6 knockout, the protein expression analysis ensured that the method was

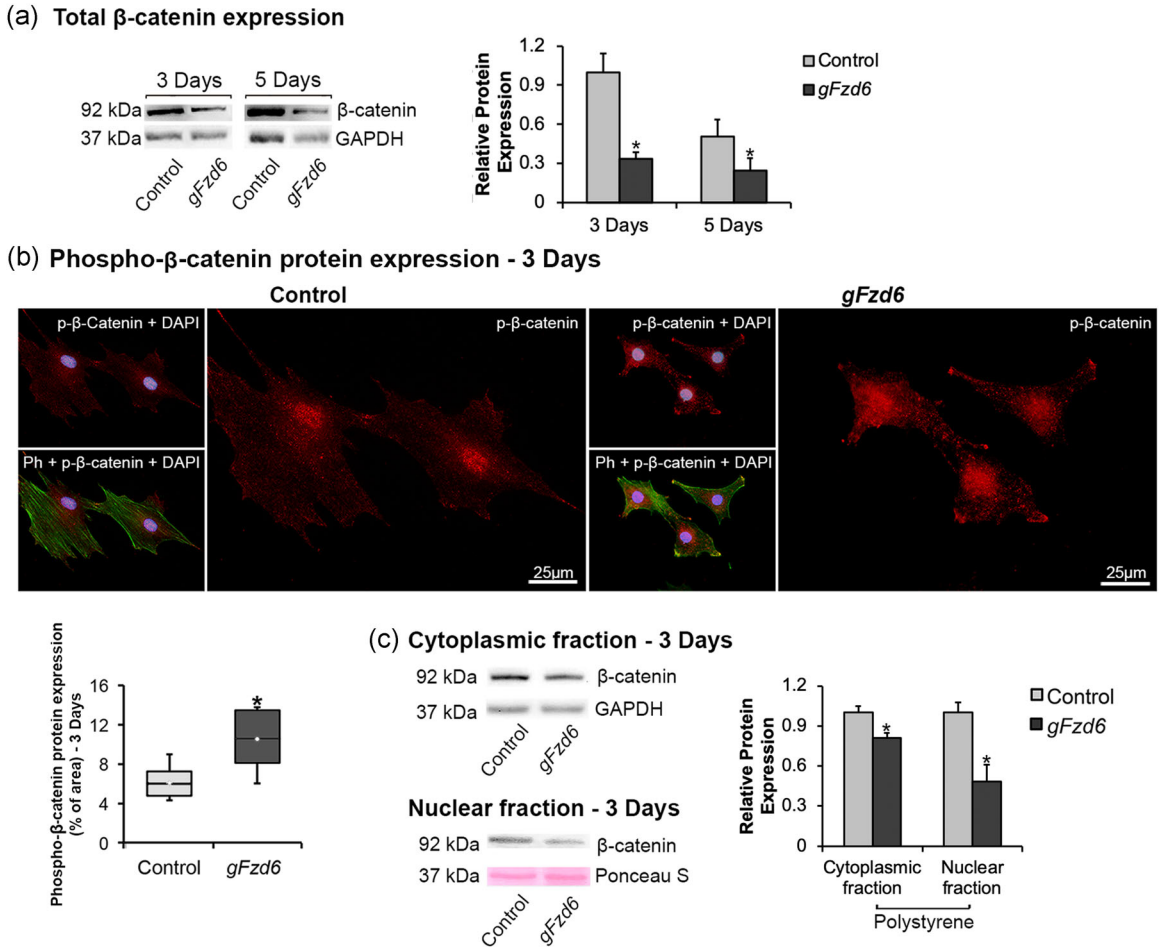

FIGURE 7 Effect of *Fzd6* silencing on the Wnt/β-catenin signaling pathway in cells grown on Ti-Nano. Protein expression of total β-catenin on Days 3 and 5 (a) and phospho-β-catenin on Day 3 (b) in MC3T3-E1 *gFzd6* and control cells grown on Ti-Nano. Total β-catenin in the cytoplasmic and nuclear fractions of *gFzd6* and control cells grown on polystyrene on Day 3 (c). Data on protein expression of phospho-β-catenin ($n = 18$) are presented as box plots. Asterisks (*) indicate statistically significant difference between control and *gFzd6* cells ($p \leq .05$). (b) Red fluorescence indicates phospho-β-catenin, green fluorescence denotes actin cytoskeleton (Phalloidin), and blue fluorescence represent cell nuclei (DAPI). FZD, frizzled; messenger RNA; Ti-Nano, titanium with nanotopography

successful, avoiding the unnecessary study of deletions or in-frame mutations (Estep, Sternburg, Sanchez, & Karginov, 2016). Therefore, we analyzed FZD6 in all surviving clones, finding one MC3T3-E1 mutated with almost undetectable FZD6 protein expression.

Limited information is available on participation of FZD6 in osteoblast phenotype development. Here, we demonstrated that FZD6 is crucial to the osteogenic response of cells grown on Ti surfaces. However, disruption reduced the levels of Runx2 in cells cultured on both surfaces and such reduction was more intense on Ti-Nano. We also observed that *Fzd6* silencing exhibited a pronounced effect on the higher osteogenicity of Ti-Nano during all stages of culture development, resulting in the reduced ALP activity and mineralization on this surface. Given that FZD6 is mainly associated with the noncanonical Wnt pathway and the high mRNA expression of *Wnt5a*, *Wnt11*, *Camk2d*, and *Camk2a* on Ti-Nano on Days 3 and 5, we started analyzing the Wnt/Ca^{2+} pathway. On microtextured Ti, Wnt5a mediated osteoblast differentiation through the Wnt/Ca^{2+} signaling (Olivares-Navarrete et al., 2011; Wall et al., 2009). On micro/nano-roughened Ti surfaces, crosstalk was observed between WNT5a and WNT11 to promote stem cell commitment into osteoblast lineage; WNT11 also mediated new bone formation and remodeling by modulating osteoclast activity and angiogenesis, suggesting a noncanonical Wnt/Ca^{2+} pathway participation (Boyan et al., 2018).

Our results revealed that phospho-CaMKII protein expression decreased from Days 3 to 5, and CaMKII protein caused no decrease after *Fzd6* silencing. Noteworthily, we observed more cells in *gFzd6* cells, suggesting that the proliferating activity is maintained by delaying the process of differentiation. CaMKII activates NFAT, which remains highly phosphorylated in the cytoplasm if not stimulated. However, any increase in calcium levels leads to the activation of calcineurin, which induces its dephosphorylation and translocation to the nucleus, in which NFAT acts as a resorption activator. However, NFATc1 and NFATc2 can also positively regulate bone formation by increasing osteoblast replication through a complex that favors the transcriptional activity of OSX (Aliprantis et al., 2008; Choi, Choi,

Oh, & Lee, 2013; Koga et al., 2005; Ueki et al., 2008). Thus, we analyzed *the Nfatc1* mRNA expression. *Fzd6* caused no decrease in its expression, suggesting that the ostegenicity of nanotopography is unrelated to the Wnt/Ca^{2+} signaling pathway activation via Fzd6 receptor.

The Fzd6 receptor may also be involved with Wnt/β-catenin signaling pathway. A positive correlation was reported to exist between *Fzd6* and Wnt/β-catenin activation in mesenchymal stem cells, in which they were upregulated after Wnt3a stimulation and repressed upon β-catenin knockdown (Kolben et al., 2012). However, *Fzd6* knockdown showed no influence on β-catenin-mediated signaling under Wnt3a stimulation, whereas the TCF/LEF-reporter assay showed a slight but nonsignificant decrease (Kolben et al., 2012). Here, *Fzd6* silencing revealed that β-catenin protein was highly affected in cells cultured on nanotopography for 3 days. In the activated status of the canonical Wnt/β-catenin pathway, the phosphorylation of β-catenin protein is reduced, as shown in our control cells. The opposite was observed in *gFzd6* cells cultured on Ti-Nano, in which phospho-β-catenin protein was increased. To confirm that Fzd6 receptor causes β-catenin-mediated signaling in these cells, we analyzed β-catenin protein expression in cytoplasmic and nuclear fractions and observed a reduced expression induced by *Fzd6* silencing in both fractions, with the reduced expression being more pronounced in the nuclear fraction. Although Fzd6 receptor is mainly associated with the noncanonical Wnt signaling pathway and may act as a negative regulator of β-catenin-dependent signaling (Frojmark et al., 2011; Golan et al., 2004), our findings expand the comprehension of Fzd6 receptor's capability to modulate Wnt/β-catenin pathway in osteoblasts grown on surfaces with nanotopography.

In conclusion, our results contribute to knowledge on the relevance of the Wnt signaling pathway to the osteoblast response to Ti surfaces. The disruption of the Fzd6 receptor inhibited the osteoblast differentiation of cells cultured on Ti-Machined and Ti-Nano. However, such inhibition was more pronounced on nanotopography, probably because the signaling pathway triggered by Fzd6 in the context of osteoblast differentiation is more influential on this surface. We have also shown that the high ostegenicity of nanotopography is, at least partially, due to the activation of the canonical Wnt/β-catenin signaling pathway triggered by Fzd6 receptor but not the noncanonical Wnt/Ca^{2+}, which is the pathway usually triggered by this receptor. These findings shed light on the biological function of Fzd6 as a gatekeeper that triggers the Wnt/β-catenin signaling pathway and expands the comprehension of the cellular mechanisms regulated by the topography of biomaterials during osteoblast differentiation.

ACKNOWLEDGMENTS

The authors would like to express thanks to Milla Sprone Tavares for her technical assistance. The English language review was carried out by ENAGO (www.enago.com) funded by FAPESP (#2018/17356-6). FAPESP (# 2016/14711-4 and 2016/14171-0), CAPES, and CNPq, (# 303464/2016-0).

CONFLICT OF INTERESTS

The authors declare that there are no conflict of interests.

AUTHOR CONTRIBUTIONS

R. P. F. A. undertook the experiments, analysed the data, and drafted and revised the manuscript; F. S. O. undertook the experiments, analysed the data and revised the manuscript; L. F. A. undertook the experiments and revised the manuscript; R. R. F. undertook the experiments and revised the manuscrip; M. M. B. designed the study, analysed the data, and drafted the manuscript; A. L. R. designed the study, analysed the data, and drafted the manuscript.

DATA AVAILABILITY STATEMENT

The data are available upon request from the corresponding author.

ORCID

Adalberto Luiz Rosa http://orcid.org/0000-0002-6495-2778

Marcio Mateus Beloti http://orcid.org/0000-0003-0149-7189

REFERENCES

Abuna, R. P. F., Oliveira, F. S., Lopes, H. B., Freitas, G. P., Fernandes, R. R., Rosa, A. L., & Beloti, M. M. (2019). The Wnt/β-catenin signaling pathway is regulated by titanium with nanotopography to induce osteoblast differentiation. *Colloids and Surfaces, B: Biointerfaces*, *184*, 110513. https://doi.org/10.1016/j.colsurfb.2019.110513

Aliprantis, A. O., Ueki, Y., Sulyanto, R., Park, A., Sigrist, K. S., Sharma, S. M., … Glimcher, L. H. (2008). NFATc1 in mice represses osteoprotegerin during osteoclastogenesis and dissociates systemic osteopenia from inflammation in cherubism. *The Journal of Clinical Investigation*, *118*, 3775–3789. https://doi.org/10.1172/JCI35711

van Amerongen, R., Mikels, A., & Nusse, R. (2008). Alternative Wnt signaling is initiated by distinct receptors. *Science Signaling*, *1*, re9. https://doi.org/10.1126/scisignal.135re9

Bilic, J., Huang, Y. L., Davidson, G., Zimmermann, T., Cruciat, C. M., Bienz, M., & Niehrs, C. (2007). Wnt induces LRP6 signalosomes and promotes dishevelled-dependent LRP6 phosphorylation. *Science*, *316*, 1619–1622. https://doi.org/10.1126/science.1137065

Bodine, P. V., & Komm, B. S. (2006). Wnt signaling and osteoblastogenesis. *Reviews in Endocrine & Metabolic Disorders*, *7*, 33–39. https://doi.org/10.1007/s11154-006-9002-4

Boyan, B. D., Olivares-Navarrete, R., Berger, M. B., Hyzy, S. L., & Schwartz, Z. (2018). Role of Wnt11 during osteogenic differentiation of human mesenchymal stem cells on microstructured titanium surfaces. *Scientific Reports*, *8*, 8588. https://doi.org/10.1038/s41598-018-26901-8

Carron, C., Pascal, A., Djiane, A., Boucaut, J. C., Shi, D. L., & Umbhauer, M. (2003). Frizzled receptor dimerization is sufficient to activate the Wnt/beta-catenin pathway. *Journal of Cell Science*, *116*, 2541–2550. https://doi.org/10.1242/jcs.00451

Castro-Raucci, L., Francischini, M. S., Teixeira, L. N., Ferraz, E. P., Lopes, H. B., de Oliveira, P. T., … Beloti, M. M. (2016). Titanium with nanotopography induces osteoblast differentiation by regulating endogenous bone morphogenetic protein expression and signaling pathway. *Journal of Cellular Biochemistry*, *117*, 1718–1726. https://doi.org/10.1002/jcb.25469

Choi, Y. H., Choi, J. H., Oh, J. W., & Lee, K. Y. (2013). Calmodulin-dependent kinase II regulates osteoblast differentiation through regulation of osterix. *Biochemical and Biophysical Research Communications*, *432*, 248–255. https://doi.org/10.1016/j.bbrc.2013.02.005

Dong, Y., Lathrop, W., Weaver, D., Qiu, Q., Cini, J., Bertolini, D., & Chen, D. (1998). Molecular cloning and characterization of LR3, a novel LDL receptor family protein with mitogenic activity. *Biochemical and Biophysical Research Communications*, *251*, 784–790. https://doi.org/10.1006/bbrc.1998.9545

Donos, N., Retzepi, M., Wall, I., Hamlet, S., & Ivanovski, S. (2011). In vivo gene expression profile of guided bone regeneration associated with a microrough titanium surface. *Clinical Oral Implants Research*, *22*, 390–398. https://doi.org/10.1111/j.1600-0501.2010.02105.x

Estep, J., Sternburg, E. L., Sanchez, G. A., & Karginov, F. V. (2016). Immunoblot screening of CRISPR/Cas9-mediated gene knockouts without selection. *BMC Molecular Biology*, *17*, 9. https://doi.org/10.1186/s12867-016-0061-0

Frojmark, A. S., Schuster, J., Sobol, M., Entesarian, M., Kilander, M. B. C., Gabrikova, D., … Dahl, N. (2011). Mutations in Frizzled 6 cause isolated autosomal-recessive nail dysplasia. *American Journal of Human Genetics*, *88*, 852–860. https://doi.org/10.1016/j.ajhg.2011.05.013

Gilbert, L. A., Larson, M. H., Morsut, L., Liu, Z., Brar, G. A., Torres, S. E., … Qi, L. S. (2013). CRISPR-mediated modular RNA-guided regulation of transcription in eukaryotes. *Cell*, *154*, 442–451. https://doi.org/10.1016/j.cell.2013.06.044

Golan, T., Yaniv, A., Bafico, A., Liu, G., & Gazit, A. (2004). The human Frizzled 6 (HFz6) acts as a negative regulator of the canonical Wnt beta-catenin signaling cascade. *The Journal of Biological Chemistry*, *279*, 14879–14888. https://doi.org/10.1074/jbc.M306421200

Gong, Y., Slee, R. B., Fukai, N., Rawadi, G., Roman-Roman, S., Reginato, A. M., … Warman, M. L. (2001). LDL receptor-related protein 5 (LRP5) affects bone accrual and eye development. *Cell*, *107*, 513–523.

Heinonen, K. M., Vanegas, J. R., Lew, D., Krosl, J., & Perreault, C. (2011). Wnt4 enhances murine hematopoietic progenitor cell expansion through a planar cell polarity-like pathway. *PLoS One*, *6*, 19279. https://doi.org/10.1371/journal.pone.0019279

Hsu, P. D., Scott, D. A., Weinstein, J. A., Ran, F. A., Konermann, S., Agarwala, V., … Zhang, F. (2013). DNA targeting specificity of RNA-guided Cas9 nucleases. *Nature Biotechnology*, *31*, 827–832. https://doi.org/10.1038/nbt.2647

Ivanovski, S., Hamlet, S., Salvi, G. E., Huynh-Ba, G., Bosshardt, D. D., Lang, N. P., & Donos, N. (2011). Transcriptional profiling of osseointegration in humans. *Clinical Oral Implants Research*, *22*, 373–381. https://doi.org/10.1111/j.1600-0501.2010.02112.x

Janda, C. Y., Waghray, D., Levin, A. M., Thomas, C., & Garcia, K. C. (2012). Structural basis of Wnt recognition by frizzled. *Science*, *337*, 59–64. https://doi.org/10.1126/science.1222879

Kato, M., Patel, M. S., Levasseur, R., Lobov, I., Chang, B. H., Glass, D. A., … Chan, L. (2002). Cbfa1-independent decrease in osteoblast proliferation, osteopenia, and persistent embryonic eye vascularization in mice deficient in Lrp5, a Wnt coreceptor. *The Journal of Cell Biology*, *157*, 303–314. https://doi.org/10.1083/jcb.200201089

Kato, R. B., Roy, B., De Oliveira, F. S., Ferraz, E. P., De Oliveira, P. T., Kemper, A. G., … Beloti, M. M. (2014). Nanotopography directs mesenchymal stem cells to osteoblast lineage through regulation of microRNA-SMAD-BMP-2 circuit. *Journal of Cellular Physiology*, *229*, 1690–1696. https://doi.org/10.1002/jcp.24614

Kestler, H. A., & Kühl, M. (2008). From individual Wnt pathways towards a Wnt signalling network. *Philosophical Transactions of the Royal Society of London, Series B: Biological Sciences*, *363*, 1333–1347. https://doi.org/10.1098/rstb.2007.2251

Koga, T., Matsui, Y., Asagiri, M., Kodama, T., de Crombrugghe, B., Nakashima, K., & Takayanagi, H. (2005). NFAT and osterix cooperatively regulate bone formation. *Nature Medicine*, *11*, 880–885. https://doi.org/10.1038/nm1270

Kolben, T., Perobner, I., Fernsebner, K., Lechner, F., Geissler, C., Ruiz-Heinrich, L., … Neth, P. (2012). Dissecting the impact of frizzled receptors in Wnt/beta-catenin signaling of human mesenchymal stem cells. *Biological Chemistry*, *393*, 1433–1447. https://doi.org/10.1515/hsz-2012-0186

Lee, H. J., Bao, J., Miller, A., Zhang, C., Wu, J., Baday, Y., … Zheng, J. (2015). Structure-based discovery of novel small molecule Wnt signaling inhibitors by targeting the cysteine rich domain of frizzled. *The Journal of Biological Chemistry*, *290*, 30596–30606. https://doi.org/10.1074/jbc.M115.673202

Lerner, U. H., & Ohlsson, C. (2015). The WNT system: Background and its role in bone. *Journal of Internal Medicine*, *277*, 630–649. https://doi.org/10.1111/joim.12368

Lopes, H. B., Freitas, G. P., Elias, C. N., Tye, C., Stein, J. L., Stein, G. S., … Beloti, M. M. (2019). Participation of integrin β3 in osteoblast differentiation induced by titanium with nano or microtopography. *Journal of Biomedical Materials Research. Part A*, *107*, 1303–1313. https://doi.org/10.1002/jbm.a.36643

MacDonald, B. T., Tamai, K., & He, X. (2009). Wnt/beta-catenin signaling: Components, mechanisms, and diseases. *Developmental Cell*, *17*, 9–26. https://doi.org/10.1016/j.devcel.2009.06.016

Mao, J., Wang, J., Liu, B., Pan, W., Farr, G. H., Flynn, C., … Wu, D. (2001). Low-density lipoprotein receptor-related protein-5 binds to Axin and regulates the canonical Wnt signaling pathway. *Molecular Cell*, *7*, 801–809. https://doi.org/10.1016/s1097-2765(01)00224-6

Mendonça, G., Mendonça, D. B., Aragão, F. J., & Coope, L. F. (2008). Advancing dental implant surface technology— from micron to nantopography. *Biomaterials*, *28*, 3822–3835. https://doi.org/10.1016/j.biomaterials.2008.05.012

Monroe, D. G., McGee-Lawrence, M. E., Oursler, M. J., & Westendorf, J. J. (2012). Update on Wnt signaling in bone cell biology and bone disease. *Gene*, *492*, 1–18. https://doi.org/10.1016/j.gene.2011.10.044

Naz, G., Pasternack, S. M., Perrin, C., Mattheisen, M., Refke, M., Khan, S., … Betz, R. C. (2012). FZD6 encoding the Wnt receptor frizzled 6 is mutated in autosomal-recessive nail dysplasia. *The British Journal of Dermatology*, *166*, 1088–1094. https://doi.org/10.1111/j.1365-2133.2011.10800.x

Olivares-Navarrete, R., Hyzy, S. L., Hutton, D. L., Dunn, G. R., Appert, C., Boyan, B. D., & Schwartz, Z. (2011). Role of non-canonical Wnt signaling in osteoblast maturation on microstructured titanium surfaces. *Acta Biomaterialia*, *7*, 2740–2750. https://doi.org/10.1016/j.actbio.2011.02.030

Olivares-Navarrete, R., Hyzy, S., Wieland, M., Boyan, B. D., & Schwartz, Z. (2010). The roles of Wnt signaling modulators Dickkopf-1 (Dkk1) and Dickkopf-2 (Dkk2) and cell maturation state in osteogenesis on microstructured titanium surfaces. *Biomaterials*, *31*, 2015–2024. https://doi.org/10.1016/j.biomaterials.2009.11.071

De Oliveira, P. T., Zalzal, S. F., Beloti, M. M., Rosa, A. L., & Nanci, A. (2007). Enhancement of in vitro osteogenesis on titanium by chemically produced nanotopography. *Journal of Biomedical Materials Research. Part A*, *80*, 554–564. https://doi.org/10.1002/jbm.a.30955

Rasouli, R., Barhoum, A., & Uludag, H. (2018). A review of nanostructured surfaces and materials for dental implants: Surface coating, patterning, and functionalization for improved performance. *Biomaterials Science*, *6*, 1312–1338. https://doi.org/10.1039/c8bm00021b

Ueki, Y., Sulyanto, R., Park, A., Sigrist, K. S., Sharma, S. M., Ostrowski, M. C., … Glimcher, L. H. (2008). NFATc1 in mice represses osteoprotegerin during osteoclastogenesis and dissociates systemic osteopenia from inflammation in cherubism. *The Journal of Clinical Investigation*, *118*, 3775–3789. https://doi.org/10.1172/JCI35711

Wall, I., Donos, N., Carlqvist, K., Jones, F., & Brett, P. (2009). Modified titanium surfaces promote accelerated osteogenic differentiation of mesenchymal stromal cells in vitro. *Bone*, *45*, 17–26. https://doi.org/10.1016/j.bone.2009.03.662

Wang, Y., Guo, N., & Nathans, J. (2006). The role of Frizzled3 and Frizzled6 in neural tube closure and in the planar polarity of inner-ear sensory hair cells. *The Journal of Neuroscience*, *26*, 2147–2156. https://doi.org/10.1523/JNEUROSCI.4698-05.2005

Yi, J. H., Bernard, C., Variola, F., Zalzal, S. F., Wuest, J. D., Rosei, F., & Nanci, A. (2006). Characterization of a bioactive nanotextured surface created by controlled chemical oxidation of titanium. *Surface Science*, *600*, 4613–4621. https://doi.org/10.1016/j.susc.2006.07.053

SUPPORTING INFORMATION

Additional supporting information may be found online in the Supporting Information section.

How to cite this article: Abuna RPF, Oliveira FS, Adolpho LF, Fernandes RR, Rosa AL, Beloti MM. Frizzled 6 disruption suppresses osteoblast differentiation induced by nanotopography through the canonical Wnt signaling pathway. *J Cell Physiol*. 2020;1–11. https://doi.org/10.1002/jcp.29674